Gold nanorod photoluminescence : applications to imaging and temperature sensing

Carattino, A.

2

In situ TUNING OF GOLD NANOROD PLASMON THROUGH OXIDATIVE CYANIDE ETCHING

Single gold nanorods exhibit great opportunities for bio-sensing, enhanced spectroscopies and photothermal therapy. A key property of these particles is the surface plasmon resonance, that is strongly dependent on their shape. Methods for tuning this resonance after the synthesis of the particles are of great interest for many applications. In this work we show that, through very well known chemistry between gold atoms and cyanide ions, it is possible to tune the surface plasmon of single 25×50 *nm rods by more than* 100 *nm towards longer wavelengths. This is achieved by slowly etching gold atoms from the surface of the particles, preserving their specific optical properties.*

This chapter has been published in Physical Chemistry Chemical Physics 18, 15619-15624 (2016).

2.1. INTRODUCTION

GOLD nanoparticles exhibit large absorption and scattering cross sections with resonances ranging from the visible to the near-infrared. This property is closely related to the surface plasmon, a collective oscillation of conduction electrons that depends on the shape of the particles. For gold nanorods (AuNR) the surface plasmon resonance (SPR) wavelength depends on the aspect ratio (AR) of the particle and can be found between 540 nm for spheres with AR of 1 to beyond 800 nm for elongated particles. The SPR of gold particles can be observed by recording their scattering or luminescence spectrum[1]. Both show a near exact overlap for a large range of wavelengths[2].

The surface plasmon presents great opportunities in (bio-) sensing[3], enhanced spectroscopies [4], photothermal therapy[5] and for concentrating light below the diffraction limit[6]. Success in many of these applications requires precise and *in situ* control over the nanoparticles' plasmon resonance energy. For example, maximum fluorescence[7] or Raman enhancement[8] is achieved when the nanoparticles' plasmon resonance is tuned to the excitation laser wavelength. As another example, efficient photothermal therapy requires the nanoparticles' SPR to be tuned to the near-IR to minimize the damage to healthy cells[9].

Typically the SPR is tuned by carefully manipulating the shapes of nanoparticles during their synthesis. Particularly useful are the rod-shaped particles, whose resonance can be found between 600 nm and beyond 1000 nm, depending on their aspect ratios. Adjusting the concentrations of gold seeds and silver nitrate during the seed-mediated growth[10] is the usual way for producing particles with different resonances. Many other nanoparticle shapes such as nanoprisms, nanorice, nanocubes, nanoshells, etc. have been synthesized with their plasmon resonances covering the entire spectral range from visible to near-IR[11]. Wet-chemical synthesis methods, however, generally yield a broad distribution in nanoparticle sizes and/or shapes, hindering precise and reproducible experiments that need a particular resonance. Furthermore, these methods do not provide any *in situ* adjustment of the SPR, any change of which requires a new synthesis.

For the past decade, single-particle experiments have provided insight into processes that would have been averaged out in bulk experiments. For instance, pump and probe experiments on single particles avoid assumptions regarding size distributions of the sample[12, 13]. Nonlinear processes such as second (or third) harmonic generation can be studied when the particles' plasmon is well characterized and single-particle experiments allow to overcome the inhomogeneous broadening of a sample in suspension[14, 15]. Enhanced spectroscopies normally rely on well defined structures fixed on a substrate[16]. Most of these experiments will benefit from techniques that allow to tune *in situ* the plasmon resonance and geometry of specific particles once they are immobilized on a substrate and optically characterized.

Recently, new methods have been developed to tune nanoparticles' SPR after their synthesis. These approaches can be divided into two broad categories: (1) The first group of methods tune the refractive index of the medium using an electric or magnetic field[17]. The advantage of these methods is that the SPR shift is reproducible and reversible. However the tuning range is rather limited and continuous tuning within this range is difficult to achieve. (2) The other set of approaches rely on controllably inducing shape modifications of the nanoparticles to tune the plasmon resonance through chemical

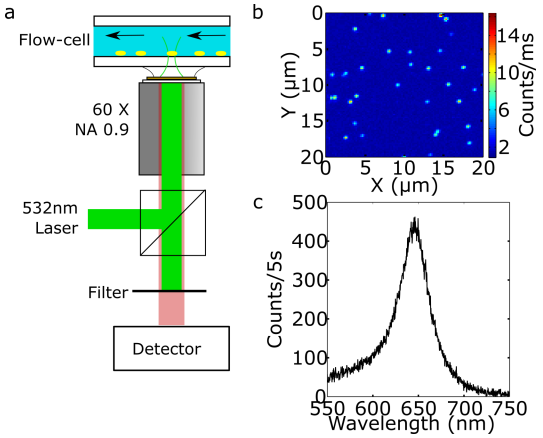

Figure 2.1: Experimental setup and examples of observations. a) Simplified schematic of the confocal microscope employed during the measurements. b) A typical 1-photon luminescence raster scan of the sample immersed in water, before etching and c) luminescence spectrum of a single rod.

or physical means. For example, thermal reshaping was induced by illuminating the nanoparticles with an intense, pulsed [18, 19] or continuous laser[2]. Increasing the particles' temperature therefore leads to changes in shape, favoring those conformations with a lower surface energy (i.e. spheres over rods, etc.). Chemical reshaping is also possible and was the focus of several studies[20–24]. In those cases, the capping agent will induce different reactivities on the sides than on the tips of the particles; because of a higher curvature[25] the tips are normally more susceptible to chemical reactions, leading to an anisotropic reshaping shortening the long axis or softening any high-curvature region. Both in the case of laser-induced or chemical-induced reshaping the outcome is usually a blue-shift of the surface resonance peak.

In this work we present a new approach for precise and *in situ* tuning of plasmon resonances of single gold nanorods isolated and immobilized on a glass surface. A nanorod's plasmon resonance is tuned over 130 nm, starting from 650 nm up to 780 nm. Our method exploits well-known chemistry between gold and cyanide ions (CN^-) to controllably etch gold atoms from the nanoparticle and thereby change its aspect ratio. We note that unlike many of the previous studies, here we observe a SPR red shift on gold nanorods. We also verified the resuts from scanning electron microscopy (SEM) images of the particles and by simulations based on the discrete dipole approximation method. Contrary to previous works where the etching was preferred at the tips, we attribute the red shift to isotropic etching of gold nanorods from all sides resulting in an increase of aspect ratio.

2.2. EXPERIMENTAL METHOD

Gold nanorods were synthesized by following standard seeded-growth method[26]. The average size of nanorods was 50 nm × 25 nm and their SPR is located at 620 nm in water (refer to the Supplementary Information for SEM images and bulk extinction spectra of nanorods as synthesized).

Single-particle measurements were done on a home-built confocal microscope (Figure 2.1a). A 532 nm laser was used for exciting the particles. The excitation power was 300 μW at the back aperture of the objective (Olympus 60×, NA 0.9 air). Since the laser employed is not in resonance with the longitudinal plasmon, the power dissipated by the particles is not high enough as for showing thermal reshaping. After several minutes of irradiation the plasmon position didn't show any shift. Typical powers needed for reshaping are in the range $1-5$ mW[2]. The luminescence signal was filtered with two 532 nm notch filters and was detected by either an avalanche photodiode or a liquid-nitrogen-cooled CCD-spectrometer (Acton 500i). The images were acquired by scanning the sample across the tightly focused laser beam using a XYZ piezo scanning stage (PI Nano Cube). Figure 2.1b shows a typical result from a raster scan. Each bright spot corresponds to a single nanoparticle.

Samples were prepared by spin-casting a suspension of AuNR on clean coverslips. Afterwards the slides were thoroughly rinsed with Milli-Q water and placed in an ozone cleaner for one hour to eliminate any trace of the surfactant (cetyltrimethylammonium bromide, CTAB.) To perform the measurements, the samples were mounted on a flowcell and the initial spectra were taken with the rods immersed in Milli-Q water. Figure 2.1c shows an example of the luminescence spectrum of a single particle. Having this initial characterization allowed us to discard clusters of rods[27] from the study.

Of each sample, approximately 10 different particles were selected. Afterwards a solution of KCN was flowed into the sample chamber and spectra of each particle were acquired consecutively after focusing on each one. The time resolution varies according to the exposure time and number of particles studied; in this work a spectrum of each particle was taken at least every minute. Concentrations of KCN ranging from 10 μM to 80 μM were employed with different samples.

2.3. RESULTS

Figure 2.1b shows a typical one-photon-excited luminescence image of gold nanorods isolated on a glass surface and covered with water. Single-particle spectra display a narrow Lorentzian lineshape[27] while clusters show additional features or a broad spectrum. Figure 2.1c shows a typical spectrum originating from a single nanoparticle. In the samples analyzed more than 90% of the diffraction-limited bright spots originate from single gold nanorods.

Figure 2.2 shows the one-photon luminescence spectra of a gold nanorod immersed in 20 μM KCN at intervals of 70 s. We clearly observe a gradual red shift of the nanorod's plasmon resonance by more than 100 nm over a time interval of 300 s. The left inset of Fig. 2.2 shows the integrated intensity of the particle as a function of time. It is possible to observe a decrease of the intensity by a factor 4 during the same interval in which the shift was observed. Fitting each spectrum with a Lorentzian function allows to extract the resonance wavelength at each recorded time. A more detailed analysis shows that the nanorod's plasmon resonance wavelength varies almost linearly with time as shown in the right inset of Fig. 2.2a

We note the presence of an additional shoulder peak at 650 nm which is more prominent for the less intense curves. We attribute this shoulder to Raman scattering by the O-H stretching modes of water, between 3000 cm^{-1} and 3600 cm^{-1}. Excitation at 532 nm

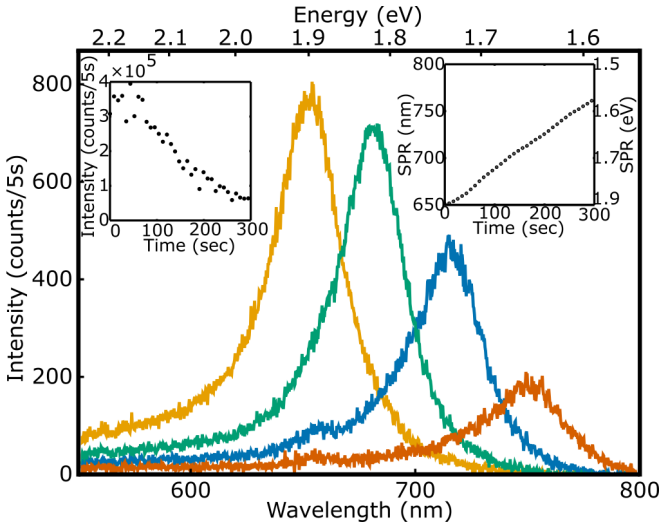

Figure 2.2: One-photon-excited luminescence spectra of gold nanorods immersed in 20 μM KCN. The different curves show the plasmon shift of a single rod. Each shown spectrum was acquired at 70 s intervals. The insets display the integrated intensity of the peak and the resonance wavelength as functions of time, respectively. b) Timetrace of the peak wavelength for 10 different particles immersed in 20 μM KCN. The green solid curve is the average of all the particles.

produces Stokes emission between roughly 630 nm and 650 nm, as observed directly on the background spectrum shown in Figure S3. This Raman band is not completely eliminated upon subtraction of the background spectrum from that of the particle. This non-additivity of the spectra indicates that water Raman scattering is significantly enhanced by the near-field of the nanorod[28].

All the studied nanorods present the same qualitative behavior. Our results are summarized in Fig. 2.3, which shows the shift of plasmon resonance wavelength as a function of time for ten different rods (dashed lines). Each nanorod shows a red shift of the plasmon resonance wavelength which varies almost linearly with time irrespective of the initial resonance wavelength. The rate of SPR shift, however, varies significantly from particle to particle. The highest observed rate was 15 nm/minute while the lowest one was 2 nm/minute. The green curve in Figure 2.3 is the average of all the shifts; since spectra of each particle were acquired sequentially, we interpolated the values of the shift at intermediate times to compute the average.

The reaction between gold and potassium cyanide is well known and is used for gold mining, electroplating, etc. Gold reacts with aqueous CN^- ions in presence of oxygen to form $Au(CN)_2^-$, which is soluble in water. The reaction can be written as follows

$$4\,Au + 8\,CN^- + O_2 + 2\,H_2O \leftrightarrows 4\,Au(CN)_2^- + 4\,OH^-$$

In our experiment the formation of $Au(CN)_2^-$ results in gold etching from the nanorods, as has been reported previously[22].

The etching of gold atoms from a nanorod has two effects: Firstly, the nanorods' volume will decrease gradually with reaction time. This is consistent with our observation

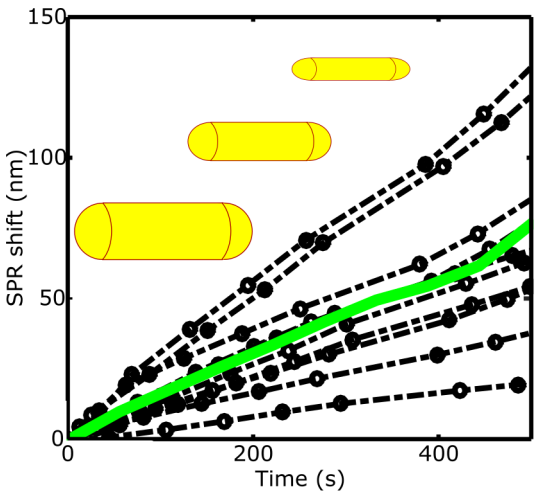

Figure 2.3: Timetrace of the peak wavelength for 10 different particles immersed in 20 μM KCN. The green solid curve is the average of all the particles. The diagram shows the isotropic etching of a nanorod, leading to a higher aspect ratio.

that the one-photon-excited luminescence intensity decreases with time. Secondly, the aspect ratio of a nanorod can either decrease or increase depending on the preferred direction of etching. The Nanorod aspect ratio will decrease with time if the reaction happens preferably at the tips. This is indeed the case for nanorods protected with CTAB and dispersed in solution[22]. CTAB binds more weakly to the tips than to the sides and therefore leaves the tips more susceptible for chemical reactions[29]. The consequent decrease of aspect ratio yields a blue shift of the plasmon resonance[30]. If etching happens isotropically from both sides and tips, an overall increase of the nanorod's aspect ratio results, as is depicted schematically in Fig. 2.3. This is the more likely scenario in our experiment as the nanorods' surface does not have any protective CTAB bilayer.

Numerical simulations based on the discrete dipole approximation were performed to assess the hypothesis that the red shift of the plasmon resonance is due to isotropic nanorod etching. The initial dimensions of the particles were fixed at 25 nm × 50 nm which coincide with the median values of the distribution of sizes of our nanoparticles (see SI). Simulations are carried out in etching steps of 0.5 nm. Figure 2.4 shows the calculated scattering spectra of the particle at different etching steps. We clearly observe a red-shift of the plasmon resonance wavelength, in concordance with what was observed in our experiment. The first inset of the figure shows the decrease of the maximum scattering cross section spectrum as a function of etched thickness.

Comparing experimental and simulated data can be achieved by fixing the value of the etching rate. In our case the best approximation to the particle shown in Figure 2.2 is achieved by setting the etching rate to 1 nm/min. Comparison to simulations for different nanorods would in principle allow us to check the consistency of the assumption of a constant etching rate for all rods. Indeed, both volume and aspect ratio of the rod can be determined by comparison of experimental data to simulations. A new comparison after

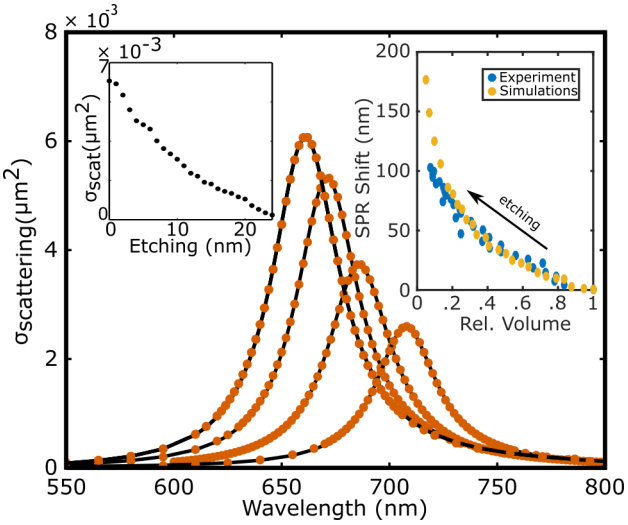

Figure 2.4: Examples of the curves obtained at different simulations steps. The black curves are fits with Lorentzians. The left inset shows the maximum scattering cross section as function of etching. The right inset displays the plasmon shift of experimental and simulated data as the relative volume of the particle diminishes.

a given etching time would give the changes in volume and aspect ratio, which should be consistent with the same etching rate for all rods. In the present work, however, we did not attempt this analysis. We simply used the relative volume as a scaling factor to compare simulations and experiments, as is shown in the right inset of Figure 2.4.

The luminescence intensity of gold nanorods is roughly proportional to their volume. It is possible therefore to calculate the relative volume of a particle by comparing the total luminescence intensity at a given instant and at a reference time. We employed the initial intensity as the reference, therefore the SPR shift increases while the relative volume decreases as depicted by the arrow in the inset of Figure 2.4. The volume of the simulated particle can be directly computed from the geometrical parameters. The inset shows a remarkable agreement between the simulations and the experimental data. For smaller relative volumes (less than 0.1) the recorded spectra are 10 times less intense than the initial one, giving rise to a less accurate positioning of the resonance peak.

Figure 2.5 shows simulated plasmon shift rates for three different series of nanorods. In each series particles have the same initial volume, but different initial plasmon resonance, spanning from 600 nm to 780 nm. The first series corresponds to 5 particles with a volume of 6800 nm^3 (red), the second to 7 particles of 20000 nm^3 (green) and the third to 6 of 25000 nm^3 (blue). The shift rate is defined as the plasmon shift given by etching a thickness of 0.5 nm away from the particle. It can be observed that for larger particles the shift is slower than for smaller ones at the same initial resonance. On the other hand it is also possible to observe that red-shifted particles present a larger shift rate.

The results in Fig. 2.5 are easier to understand considering that the plasmon resonance is closely related to the aspect ratio of the particles (length divided by diameter). Small particles will exhibit a bigger change in aspect ratio when subjected to the same amount

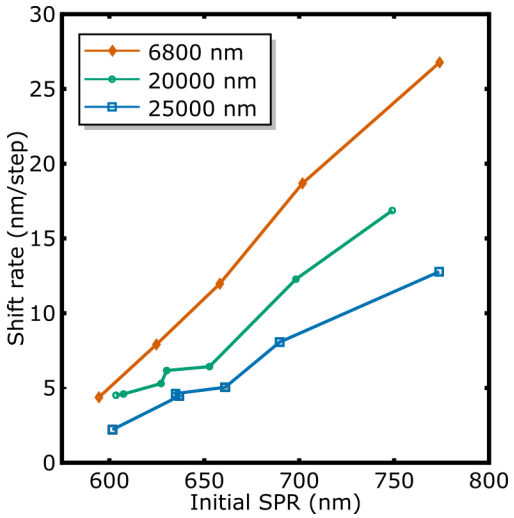

Figure 2.5: Shift rate as a function of the initial plasmon resonance for different particles. The lines correspond to particles with the same initial volume but different initial aspect ratios. As expected from an isotropic etching, larger particles will present a slower plasmon shift and more elongated particles will have a faster one.

of etching than bigger particles. This explains why smaller particles show a higher shift rate than more massive ones. On the other hand, volume is not the only factor to take into account. Particles with a higher initial aspect ratio (longer resonance wavelength) will show a faster change in aspect ratio when subjected to the same amount of etching. The interplay between both volume and initial aspect ratio can account for the big variability observed experimentally. This is also supported by the distribution of particle sizes and aspect ratios observed in the SEM images (see A.2.)

Figure 2.6 shows the measured FWHM of the plasmon peak for several nanorods immersed in 20 μM KCN as a function of the resonance shift. Note that the plot shows the width of the resonance in units of energy and not in units of wavelength. Because of the nonlinear relation between them, the peak width expressed in wavelength depends on the peak position rendering difficult the comparison of widths during the shift. At the beginning of the reaction there is a decrease of the width. Then it stabilizes for shifts between 75 nm and 100 nm. After this point, as the volume of the particles is largely reduced, it is no longer possible to reliably extract information from the spectra. The inset of Fig. 2.6 shows the FWHM obtained from the simulations for a 25 nm × 50 nm nanorod. The simulated spectrum is slightly narrower than the measured one but the trends are similar.

The initial decrease of the resonance FWHM observed in the experiments may be due to the elimination of defects from the surface of the particles. However, the simulated width that doesn't take into account any surface impurities shows a similar decrease. This behavior can be explained by the decrease of both the radiative and non-radiative damping mechanisms during the etching process. The radiation damping scales as the volume of the particle[31] and therefore will decrease while the cyanide etches gold atoms

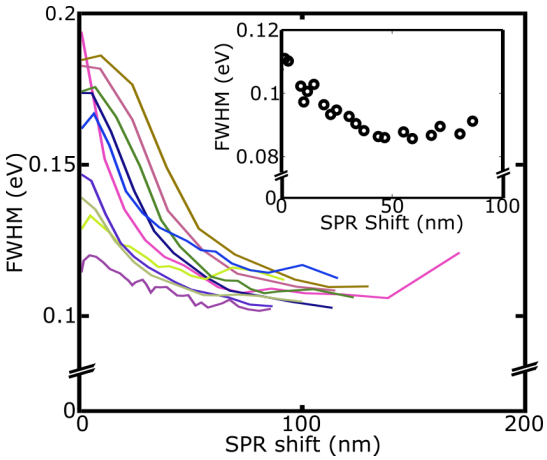

Figure 2.6: Measured plasmon FWHM of different particles immersed in 20 μM KCN as a function of their plasmon shift. The inset shows the results from the simulations carried out with the ADDA package. b) SPR Shift as a function of time for particles with the same initial SPR at different KCN concentrations.

from the particle. On the other hand we observe that the energy distance between the longitudinal plasmon peak and interband transitions in gold increases during the etching process. Therefore the non-radiative damping mechanisms in the particle may also become less efficient[1]. Both effects combined can account for the diminishing plasmon width that is observed.

Figure 2.7 shows the plasmon peak shift as a function of time for various KCN concentrations for particles with a plasmon peak at roughly 630 nm. As shown for the simulations (Figure 2.5), the etching rate depends on the initial SPR, therefore it is important to choose particles that are similar to each other. The time-traces of the peak position clearly show that the shift rate is proportional to the concentration of KCN. For every concentration a shift of at least 100 nm was observed. It is important to note that the behavior of the FWHM in all the cases is similar and it resembles the results shown in Figure 2.7.

Samples of the same nanorods were prepared for scanning electron microscopy (SEM) imaging by drop-casting the same solution of rods. SEM images were acquired before the etching, after 2 min immersion in KCN and after 4 min. In each case we observed that when particles are isolated from each other, the rod shape is preserved. In aggregates of particles this no longer holds and rods start to lose their shape (see Supporting Information for SEM images.) Calculating the distribution of sizes of the particles shows a slight increase in the aspect ratio but this shift is smaller than the width of the distribution.

The simulations also allow us to estimate the volume of gold etched away from a particle by unit of time. For a typical case as the one depicted in Figure 2.7 it is possible to obtain an etching rate of 0.5 nm/ min for the 10 μM timetrace. Assuming an atomic radius of gold of 144 pm[32] we obtain that the reaction rate can be as low as 700 atoms per second. From the simulations and these estimates it is possible to approximate the plasmon shift for every etched atom. In the same conditions as before, it would be $0.2 \cdot 10^{-3}$ nm/atom, several orders of magnitude smaller that the sensitivity of our

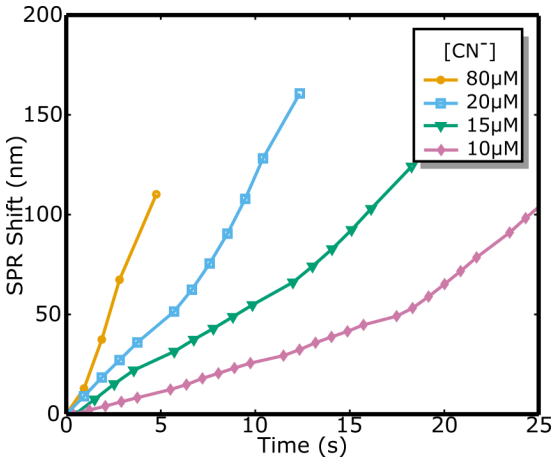

Figure 2.7: SPR Shift as a function of time for particles with the same initial SPR at different KCN concentrations.

experiments.

The same experiments performed in solution (see SI) show a different behavior of the plasmon resonance. As reported by other groups [22, 25] the rods reshape into spheres. The presence of CTAB can explain this trend: the tips will be more exposed and therefore react more quickly, yielding a net decrease in aspect ratio. In our single-particle experiments CTAB was removed both by rinsing the samples with water and by placing them in an ozone cleaner. However, the glass surface supporting the rods has to be taken into account. In principle there is a side of the rods in contact with the surface that will be less, or not, exposed to KCN. Etching in this case wouldn't be isotropic and would flatten the rods. Neither the optical nor the SEM images allowed us to assess this question because there is no information on the axis perpendicular to the surface. The deviation of the experiments from the simulations for the smaller volumes may be also dependent on this.

2.4. CONCLUSIONS

In this work we have shown a simple method that allowed us to tune the plasmon peak position of single gold nanorods with nanometer accuracy and over the range of 100 nm (300 meV). More importantly, we show that during the etching process the rod-like shape is preserved; this was confirmed both by monitoring the FWHM of the resonance peak and by acquiring SEM images after different reaction times. The experiments allowed us to record the plasmon peak with a relatively high temporal and spectral accuracy, allowing us to stop the reaction when the resonance is at the desired value.

Discrete dipole simulations with an isotropic etching model allowed us to estimate the amount of gold etched from the nanoparticles. The calculations were consistent with the red-shift of the plasmon and the diminishing intensity of the luminescence signal. The general trend of the FWHM is also correctly reproduced, but the obtained values are slightly different. SEM images of the rods confirmed the values obtained from the

simulations. Combining these results provides a way of predicting the behaviour of the plasmon peak for different rods.

We observed a broad distribution of the rate at which the plasmon peak shifts for different particles under the same experimental conditions. This can be attributed to the initial differences in aspect ratios and volumes of each particle. Sphere-like particles will show a small shift since the aspect ratio remains constant under isotropic etching. More elongated particles, on the other hand, will have a much steeper increase in aspect ratio while being etched. Intrinsic differences between particles can also be present, producing different shift rates even if particles have the same plasmon resonance. For instance the faceting of the surface or the prescence of left-over CTAB that was not completely washed away or oxidized can induce a slightly anisotropic etching. These differences between particles are impossible to assess by optical means and would require a much more sensitive approach.

The role of the capping agent has largely been studied and has always been held responsible for the observations both in chemical etching[25] and for photothermal reshaping[19]. Avoiding the presence of the passivating layers is impossible in suspension, since gold nanoparticles would aggregate. Our results provide evidence that supports previous observations regarding the effect of the curvature and the accessibility of KCN to the surface of the particle.

REFERENCES

[1] C. Sönnichsen, T. Franzl, T. Wilk, G. von Plessen, J. Feldmann, O. Wilson, and P. Mulvaney, *Drastic Reduction of Plasmon Damping in Gold Nanorods,* Phys. Rev. Lett. **88**, 077402 (2002).

[2] M. Yorulmaz, S. Khatua, P. Zijlstra, A. Gaiduk, and M. Orrit, *Luminescence quantum yield of single gold nanorods.* Nano Lett. **12**, 4385 (2012).

[3] P. Zijlstra, P. M. R. Paulo, and M. Orrit, *Optical detection of single non-absorbing molecules using the surface plasmon resonance of a gold nanorod.* Nat. Nanotechnol. **7**, 379 (2012).

[4] S. T. Sivapalan, B. M. Devetter, T. K. Yang, T. van Dijk, M. V. Schulmerich, P. S. Carney, R. Bhargava, and C. J. Murphy, *Off-resonance surface-enhanced Raman spectroscopy from gold nanorod suspensions as a function of aspect ratio: not what we thought.* ACS Nano **7**, 2099 (2013).

[5] T. Zhao, K. Yu, L. Li, T. Zhang, Z. Guan, N. Gao, P. Yuan, S. Li, S. Q. Yao, Q.-H. Xu, and G. Q. Xu, *Gold nanorod enhanced two-photon excitation fluorescence of photosensitizers for two-photon imaging and photodynamic therapy.* ACS Appl. Mater. Interfaces **6**, 2700 (2014).

[6] P. Zijlstra and M. Orrit, *Single metal nanoparticles: optical detection, spectroscopy and applications,* Reports Prog. Phys. **74**, 106401 (2011).

[7] S. Khatua, P. M. R. Paulo, H. Yuan, A. Gupta, P. Zijlstra, and M. Orrit, *Resonant plasmonic enhancement of single-molecule fluorescence by individual gold nanorods.* ACS Nano **8**, 4440 (2014).

[8] A. D. McFarland, M. a. Young, J. a. Dieringer, and R. P. Van Duyne, *Wavelength-scanned surface-enhanced Raman excitation spectroscopy.* J. Phys. Chem. B **109**, 11279 (2005).

[9] A. M. Alkilany, L. B. Thompson, S. P. Boulos, P. N. Sisco, and C. J. Murphy, *Gold nanorods: Their potential for photothermal therapeutics and drug delivery, tempered by the complexity of their biological interactions,* Adv. Drug Deliv. Rev. **64**, 190 (2012).

[10] L. Vigderman, B. P. Khanal, and E. R. Zubarev, *Functional gold nanorods: Synthesis, self-assembly, and sensing applications,* Adv. Mater. **24**, 4811 (2012).

[11] S. Lal, S. Link, and N. J. Halas, *Nano-optics from sensing to waveguiding,* Nat. Photonics **1**, 641 (2007).

[12] G. V. Hartland, *Coherent Excitation of Vibrational Modes in Metallic Nanoparticles,* Annu. Rev. Phys. Chem. **57**, 403 (2006).

[13] P. V. Ruijgrok, P. Zijlstra, A. L. Tchebotareva, and M. Orrit, *Damping of acoustic vibrations of single gold nanoparticles optically trapped in water.* Nano Lett. **12**, 1063 (2012).

[14] J. Butet, J. Duboisset, G. Bachelier, I. Russier-Antoine, E. Benichou, C. Jonin, and P. F. Brevet, *Optical second harmonic generation of single metallic nanoparticles embedded in a homogeneous medium,* Nano Lett. **10**, 1717 (2010).

[15] M. Lippitz, M. A. Van Dijk, and M. Orrit, *Third-harmonic generation from single gold nanoparticles,* Nano Lett. **5**, 799 (2005).

[16] P. Olk, J. Renger, M. T. Wenzel, and L. M. Eng, *Distance dependent spectral tuning of two coupled metal nanoparticles,* Nano Lett. **8**, 1174 (2008).

[17] P. A. Kossyrev, A. Yin, S. G. Cloutier, D. a. Cardimona, D. Huang, P. M. Alsing, and J. M. Xu, *Electric field tuning of plasmonic response of nanodot array in liquid crystal matrix,* Nano Lett. **5**, 1978 (2005).

[18] S. Link, C. Burda, B. Nikoobakht, and M. A. El-Sayed, *Laser-Induced Shape Changes of Colloidal Gold Nanorods Using Femtosecond and Nanosecond Laser Pulses,* J. Phys. Chem. B **104**, 6152 (2000).

[19] Y. Horiguchi, K. Honda, Y. Kato, N. Nakashima, and Y. Niidome, *Photothermal reshaping of gold nanorods depends on the passivating layers of the nanorod surfaces,* Langmuir **24**, 12026 (2008).

[20] E. Carbó-Argibay, B. Rodríguez-González, J. Pacifico, I. Pastoriza-Santos, J. Pérez-Juste, and L. Liz-Marzán, *Chemical Sharpening of Gold Nanorods: The Rod-to-Octahedron Transition,* Angew. Chemie **119**, 9141 (2007).

[21] J. Rodríguez-Fernández, J. Pérez-Juste, P. Mulvaney, and L. M. Liz-Marzán, *Spatially-directed oxidation of gold nanoparticles by Au(III)-CTAB complexes.* J. Phys. Chem. B **109**, 14257 (2005).

[22] N. R. Jana, L. Gearheart, S. O. Obare, and C. J. Murphy, *Anisotropic Chemical Reactivity of Gold Spheroids and Nanorods,* Langmuir **18**, 922 (2002).

[23] C. K. Tsung, X. Kou, Q. Shi, J. Zhang, M. H. Yeung, J. Wang, and G. D. Stucky, *Selective shortening of single-crystalline gold nanorods by mild oxidation,* J. Am. Chem. Soc. **128**, 5352 (2006).

[24] W. Ni, X. Kou, Z. Yang, and J. Wang, *Tailoring longitudinal surface plasmon wavelengths, scattering and absorption cross sections of gold nanorods,* ACS Nano **2**, 677 (2008).

[25] H. Yuan, K. P. F. Janssen, T. Franklin, G. Lu, L. Su, X. Gu, H. Uji-i, M. B. J. Roeffaers, and J. Hofkens, *Reshaping anisotropic gold nanoparticles through oxidative etching: the role of the surfactant and nanoparticle surface curvature,* RSC Adv. **5**, 6829 (2015).

[26] B. Nikoobakht and M. A. El-Sayed, *Preparation and Growth Mechanism of Gold Nanorods (NRs) Using Seed-Mediated Growth Method,* Chem. Mater. **15**, 1957 (2003).

[27] A. M. Funston, C. Novo, T. J. Davis, and P. Mulvaney, *Plasmon coupling of gold nanorods at short distances and in different geometries,* Nano Lett. **9**, 1651 (2009).

[28] J. B. Snow, S. X. Qian, and R. K. Chang, *Stimulated Raman scattering from individual water and ethanol droplets at morphology-dependent resonances.* Opt. Lett. **10**, 37 (1985).

[29] K. K. Caswell, J. N. Wilson, U. H. F. Bunz, and C. J. Murphy, *Preferential end-to-end assembly of gold nanorods by biotin- streptavidin connectors,* J. Am. Chem. Soc. **125**, 13914 (2003).

[30] S. Link, M. B. Mohamed, and M. a. El-Sayed, *Simulation of the Optical Absorption Spectra of Gold Nanorods as a Function of Their Aspect Ratio and the Effect of the Medium Dielectric Constant,* J. Phys. Chem. B **103**, 3073 (1999).

[31] a. Wokaun, J. P. Gordon, and P. F. Liao, *Radiation damping in surface-enhanced Raman scattering,* Phys. Rev. Lett. **48**, 957 (1982).

[32] L. Pauling, *Atomic Radii and Interatomic Distances in Metals,* J. Am. Chem. Soc. **69**, 542 (1947).